Design of Adaptive Optics System for Terrestrial Surveillance

Joshua W. Friend[1]

University of New South Wales at the Australian Defence Force Academy

Adaptive optic systems have been successfully implemented in astronomy applications to counteract the effects of atmospheric distortion. There is relatively little research in the application of adaptive optics in the area of terrestrial surveillance. This research project aimed to design an adaptive optics system for terrestrial surveillance. The performance of individual components were characterised in order to optimise system performance. Field testing indicates that a quadrature photodiode is able to adequately map wavefront distortion over 185m range at night. The level of atmospheric distortion was able to be mapped to a range of ±1.5mm lateral displacement. The designed PID controller algorithm was shown to be accurate for a range of PID controller variants. The implemented data collection functionality enabled the post processing of experimental results to aid system development. The results obtained will guide the further development of the system as a correctional mirror is implemented to complete the control system design.

Contents

[1]SBLT, School of Engineering & Information Technology. ZEIT4501

I. Introduction

Modern optical systems are able to be constructed with sufficient precision such that the image quality is diffraction limited; meaning that the quality and resolution of received images are not affected by imperfections in the fabrication of the optical system itself. As such the limiting factor of the resolution is in the size of the lenses utilized in the system. Despite this these systems do not achieve the theoretical level of performance due to the quality of the incoming wave fronts of light. The incoming light is distorted whilst travelling through the medium of transmission, resulting in distortion due to phase aberrations of the received image in the optical system. As such by necessity efforts to improve the performance of an optical system must incorporate efforts to counteract this distortion. The field of Adaptive Optics is the branch of optics that implements a range of techniques to actively compensate for the phase aberrations of incoming light [2].

The phase aberrations are derived from the nature of the medium of transmission of the light. In terrestrial surveillance and astronomy implementations this is the Earth's atmosphere. Whilst the phase aberrations introduced by the Earth's atmosphere are due to a number of different atmospheric conditions, the primary mechanism of distortion is the transmission of light through pockets of air with differing refractive indexes [3]. Merkle (1991) notes these pockets of air are caused by wind mixing air of differing temperatures. It is also noted that the presence of convection air currents contribute significantly to ground level atmospheric distortion in a similar manner [3]. The dynamic nature of the atmosphere results in the temporal evolution of the distortion. When compared with the distortion seen in astronomy implementations Lambert et al (2008) notes that surveillance imaging close to the ground during the day is expected to exhibit not only more significant distortion but also more rapid evolution of the distortion [4]. As such it can be seen that the implementation of an adaptive optics system for a Terrestrial Surveillance provides significant challenges that are not extant for astronomy implementations.

II. Project Description

This project will involve the design and development of the individual components required to construct a simple adaptive optics system for use in terrestrial surveillance. The adaptive optics system is to be implemented for an extant military telescope. This telescope has a focal length of 2m with a reflecting mirror diameter of 0.14m. The system must be able to effectively be integrated onto this platform without the requirement for permanent modification and impairment of system operation. The design aims to provide a proof of concept developmental system that is able to provide a degree of correction for the distortion introduced by the ground layer turbulence. The design process will include the characterisation of system components to provide a foundation for future modifications and development. Testing of subsystems individually will be conducted in order to provide quantitative analysis of system performance.

III. Aims

The aim of this report is to document the tip/tilt adaptive optics system built throughout the project. This will include presenting an analysis of the development of the adaptive optics subsystem components and the effectiveness of these systems to meet the requirements of an adaptive optics system for terrestrial surveillance. This will include the characterisation of the individual components within the subsystem, and the subsystem as a standalone system. This will highlight the effect of the individual components on the subsystem performance in order to provide a complete description of the system operation. The effectiveness of these components will be assessed against implementation on the identified optical platform for terrestrial surveillance.

IV. Adaptive Optics System Description

Any adaptive optics system must include three base components; a wave front sensor, correctional mirror and control system. More complex systems utilise multistage corrections applying different components for each of these stages. This project aims to implement a simple, single stage correction for the incoming light. This drove the decision behind the selection of components in the design of the subsystems.

A. Constraints

The constraints for this project are determined by the configuration of the optical system and the expected and experimentally derived levels of atmospheric turbulence. These factors give the requisite levels of performance required in terms of speed of operation of the control system and speed and range of the wavefront

sensor and correctional mirror. Specific constraints for sub systems will be duly documented throughout the report.

B. Correctional Mirror

Correctional mirrors correct for the phase aberrations of the incoming wave front by changing the length of the optical path taken by the light through the optical system [5]. There are two main types of correctional mirrors that are utilised; tip/tilt mirrors and deformable mirrors. Tip/tilt mirrors are mirrors that are able to be moved in two planes in order to compensate for wave front tilts. Due to their high stroke they are commonly utilized as an initial stage correction, allowing further higher-order corrections to be made by deformable mirrors. Deformable mirrors are composed of a flexible reflective surface that is able to be selectively deformed to correct the high order aberrations of the incoming wave front.

C. Wave Front Sensor

The purpose of the wave front sensor is to detect the phase aberrations of the incoming wave fronts and passing these in a suitable manner to the control system. The main device utilized in astronomy implementations is a Shack-Hartmann sensor [6]. This device uses a micro-lens array to focus segments of the incoming wave front onto an array of photo-detecting devices. The relative position of the focused wave front on each photo-detector is able to be used to calculate the slope of the incoming wave front [3]. This form of wave front detector is commonly used in conjunction with a deformable mirror. Simpler schemes can be implemented for broader corrections implementing single photo-detecting elements. Literature identifies two main components that are utilised as the photo-sensing component of the wave front sensor in adaptive optics systems, being quadrature photodiodes and charge coupled devices (CCDs) [7].

D. Control System

The control system for an adaptive optics system is responsible for taking the raw output of the wave front sensor and turning that into an accurate representation of the phase aberrations of the incoming wave front. Once this is achieved the control algorithm is processed in order to determine the movement of the correctional mirror to compensate for the wave front aberrations. For implementations utilizing Shack-Hartmann sensors the calculations required to determine the slope of the wave front is computationally significant in order to meet the speed and spatial sampling requirements [3].

E. Designed System

The project aim of providing a proof of concept system heavily influenced the selection of components for the aforementioned subsystems. It was identified that the achievement of broad corrections should improve the performance of the optical system and as such meet the project aims. As such a system of the lowest overall complexity was chosen.

A tip/tilt mirror was identified as the correctional mirror under consultation with Dr Lambert early on due to cost and resources restrictions. This required only the overall slope of the wave front to be detected, as opposed to the changing slope within the wave front. Whilst this information can be extracted from a Shack-Hartmann, a single photo detector device is able to provide the same information with less computational effort, cost and system complexity. As such an appropriately biased quadrature photodiode was utilised as the wave front sensor for this project. Similarly the computational effort required to drive a tip/tilt mirror is significantly lower than that of deformable mirrors, allowing a microprocessor to be utilised to implement the control system.

An Arduino class microprocessor, ATmega 16U4, in the PJRC form factor Teensy 2.0 was identified as an appropriate device to implement the control system. The control system itself was implemented utilising a PID controller. PID controllers are implemented in a wide range of applications throughout industry due to the flexibility of their implementation and ease of tuning [8]. As such there is a broad range of resources available that reduced the risk with successful implementation of the system.

V. Background Theory

A. Photodiode Operation

A photodiode is a P-N junction diode that generates a photocurrent that is proportional to the number of photons absorbed by the active area of the device [9]. The photodiode can be operated in two modes of operation; photoconductive and photovoltaic.

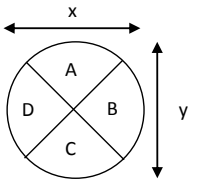

$$L_x = \frac{A - C}{A + C}$$

$$L_y = \frac{B - D}{B + D}$$

Figure 1: Orientation of Quadrature Photodiode

Photovoltaic mode requires no bias to be applied to the diode, making the depletion zone as small as possible, thus making it suitable to ultra-low light, yet slow implementations [9]. Photoconductive mode significantly improves the speed and linearity of the device and as such was the selected mode of operation for this project.

A SPOT-4D quadrature photodiode from OSI optoelectronics was utilised to realise the wave front sensor [10]. The use of a single photodiode as the wave front sensor utilises the principle of a 'guide star' pioneered in 1987 in astronomy implementations [11]. This utilises a point source near or close to the target which is able to be focused onto the centre of the quadrature photodiode. As such the reference point moves across the active area of the photodiode differing levels of photocurrent will be generated. This means that the effective movement, and resulting phase aberrations of the incoming wave fronts can be mapped by tracking the changes in the currents generated in each of the photodiode quadrants.

This can be implemented practicably through the projection of a laser onto the target, as this provides a guide spot that is uniform in intensity. The guide spot utilised for the field testing was a white LED fitted with a collimator.

B. Controller Theory

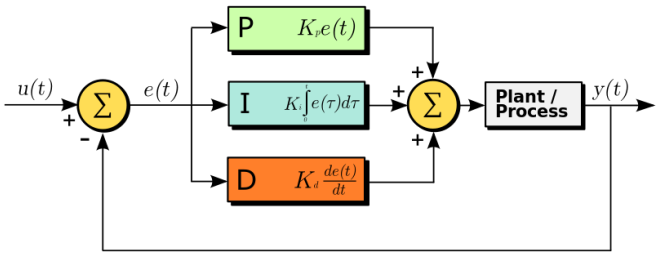

$$CO = CO_{bias} + K_p e(t) + K_I \int e(t)dt + K_D \frac{de(t)}{dt}$$

CO = Control Output
PV = Process Variable
SP = Setpoint
e(t) = SP − PV
CO_{bias} = Controller bias

Figure 2: Structure of PID controller [1]

A PID controller is a control system that achieves control of a system through iterative calculations of an error value between a measured process variable and defined set point. The PID algorithm involves three main variables describing the contribution of proportional, integral and derivative control to the system, denoted by K_P, K_I and K_D respectively. These parameters effectively determine the degree to which the control system implements that attribute in the calculation of the output.

Kp contributes to the output dependent on the current error level, whilst Ki contributes to the controller output dependent on the integral, or the sum of past errors, and Kd contributes to the controller output dependent on future errors, as predicted by the current rate of change of the error. These values must be tuned with respect to the transfer function of the plant in order to optimise the response of the system.

One significant advantage of the PID controller is that it can be tuned online without explicit knowledge of the transfer function of the plant. In addition, there exists a number of tried and tested tuning methods that are able to be implemented such as the Zieger-Nichols tuning method, frequency-response approach and computational optimisation [8].

C. Arduino Microprocessor

The Arduino Teensy 2.0 microcontroller utilized an ATmega16U4 8 bit AVR microprocessor to implement the microcontroller system [12]. This chip provides a number of inbuilt functions that were exploited in the design of the control system- namely the inbuilt timers, hardware interrupts and on-board ADC converters. The processor also presented significant issues due to the limited resources available, with only 32kB of flash memory and a maximum clock speed of 16MHz [13].

VI. Design and Development

A. Wave Front Sensor Design

In order to implement the quadrature photodiode as a wave front sensor an appropriate biasing circuit had to be implemented. This is in order to ensure the photodiode performed reliably and provides the control system with a suitable input. When this was achieved the system was characterised in order to be able to quantitatively analyse its performance and identify limiting factors within the system. The main factors considered when characterising the subsystem were Signal-Noise Ratio (SNR), linearity of the circuit, the effect of reverse bias on the output and most importantly, the slew rate.

Datasheets and literature provide consistent examples of methods of biasing a photodiode in photoconductive mode [9, 10, 14]. All designs implement operational amplifiers in order to convert the current produced by the photodiode to a voltage. The final design implemented is attached in Appendix A1.

1. Reverse Bias

The reverse biasing of the photodiode ensures that the device is operating in photoconductive mode and has a number of desirable advantages for this implementation. The linearity of the device is extended for a wider range of incident light levels when reverse bias is applied [9]. The main improvement in performance is derived from the decrease in junction capacitance due to the reverse bias. The junction capacitance is inversely proportional the speed of the device. This results in an increase in the speed of the device as a greater reverse bias is applied to the diode, proportional to the relative junction capacitance as shown in figure 3.

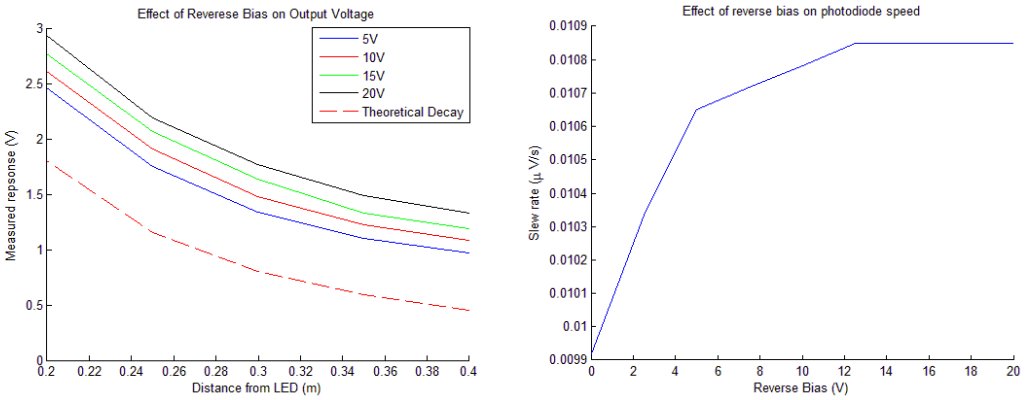

Figure 3: Experimentally derived effects of reverse bias on photodiode performance and sensor output for reverse bias over range of distances from light source (*left*), and effect of reverse bias on speed of photodiode (*right*).

2. Linearity

As discussed, linearity of the device is important to ensure predictable operation of the wave front sensor over the range of incident light intensities. The light intensity is expected to exhibit inverse square decay assuming spherical propagation from the source LED. Testing was conducted with a constant source intensity measured at set distances confirmed the predicted inverse square decay of measured intensity as shown in figure 3.

3. SNR

Experimental measurement of the noise of the wave front sensor was shown to be relatively constant across the tested frequencies at 6µV. This was identified to be just above the ADC resolution of 4.9µV. Whilst the SNR displayed a linear relationship as demonstrated in figure 4, different values of capacitors were tested to determine the effectiveness of the filtering provided in order to reduce the extant noise below the ADC resolution. It was observed that there was a reduction of approximately 2µV in the noise level when a 10pF capacitor was introduced into the op-amp feedback loop. This reduction in noise was observed to be constant irrespective of the capacitor value. This factor allowed an additional degree of freedom within the design as it permitted a variety of capacitor values that effectively decreased the noise to an acceptable level.

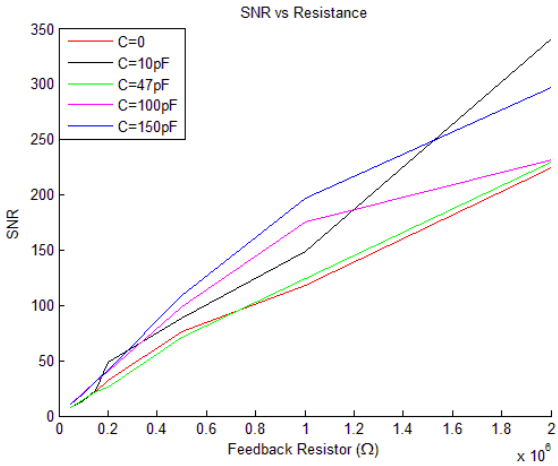

Figure 4: SNR for different RC combinations

4. Extant noise in the system

Literature states that the dominant noise source for the photoconductive mode is shot noise, which is proportional to the photocurrent and reverse bias applied to the photodiode [15]. It was observed that an increase in reverse bias did not result in a perceptible level of noise in the measured data, and as such it was deduced that the majority of noise was due to other factors. In addition to the thermal noise extant in the system, variations within the reference voltage and reverse bias for the photodiode contribute to the noise floor. In order to quantify the level of noise expected within the system the performance of the reference and biasing voltages were analysed.

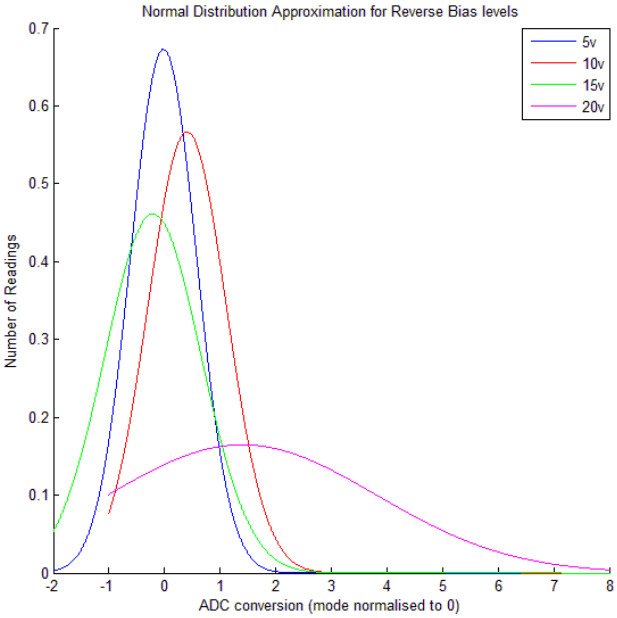

Figure 5: Variance of different reverse bias voltages

It is noted that the ADC of the ATmega16U4 exhibits an accuracy of ± 2 LSB, thus introducing an inherent and unavoidable source of noise [13]. In addition it was demonstrated that there was variance in the voltage utilised to generate the bias to the photodiode. As demonstrated in figure 5, the reverse bias is proportional to the output voltage, and as such fluctuations in the reverse bias voltage would impact the measured results. As shown in figure 5 the noise of the DC power supply was proportional, with higher voltages exhibiting higher levels of variance. The lower levels of bias can be seen to fall within the limits of the ADC accuracy and as such can be implemented without effect. However the upper levels of 15-20V were found to produce results out of this range, thus introducing noise into the system. The voltage reference of Atmega16U4 showed good consistency with variation within the limits of the ADC's accuracy constraints.

5. Slew Rate

This circuit effectively forms a current driven low-pass filter in the first op-amp stage. Due to this it was identified that the RC combination of the biasing circuit had to be small enough to ensure the limiting factor in circuit speed was the sampling frequency of the inputs. This is able to be quantified in the relationship shown below:

$$\frac{1}{2\pi RC} > \frac{f_s}{2}$$

As the slew rate of the system is determined by the component with the lowest individual slew rate, the slew rate of the implemented operational amplifier, inverting gain stage and biased circuit were evaluated

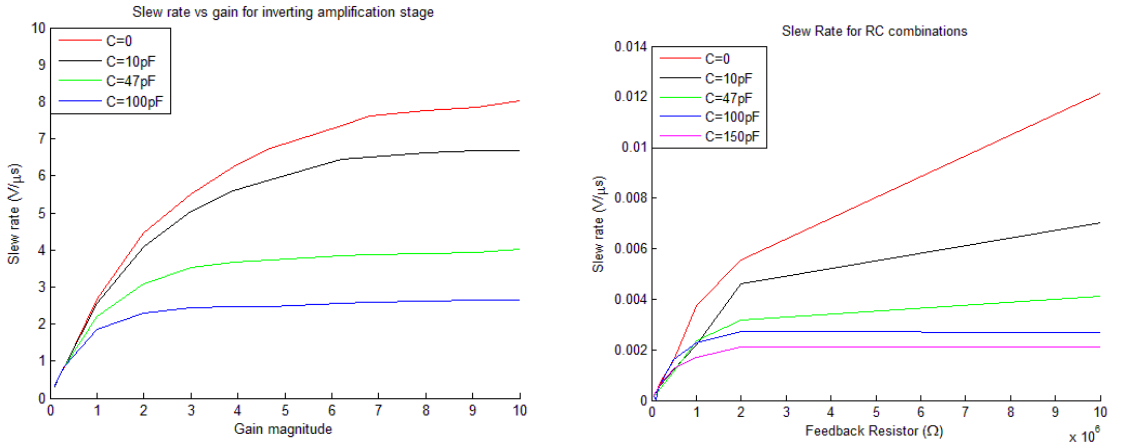

Figure 6: Slew Rate for inverting gain stage (*left*), Slew rate for different RC combinations (*right*)

individually. This approach allowed for the identification of the effective bottleneck in the system design enabling design trade-offs to be considered in order to maximise the system performance. The TL074 was chosen due to its advertised and experimentally confirmed high slew rate of 8-13 V/μs [16]. Experimental results determined that the photodiode was the limiting factor for the wavefront sensor, with the experimentally derived slew rate being significantly lower than that of the other circuit components. This also showed that the slew rate was dependent on the on the RC combination in the feedback of the op-amp. The slew rate limits the speed dependant on both the magnitude and frequency of the distortion. As such for larger levels of atmospheric distortion the photodiode will only be able to accurately follow lower temporal evolutions.

6. Implementation considerations

There are several physical limitations to the implementations of this wavefront sensor in terms of interaction with the guide spot. The guide spot must be focussed on the centre of the photodiode, implemented through the use of a beam splitter to direct a portion of the incoming light to the wavefront sensor. The size of the guide spot must be sufficiently large to overlap all segments for all levels of distortion, consequently it cannot be smaller than the spacing between the photodiode segments [9]. Similarly it must be small enough that for all distortions experienced the light spot must remain on the photodiodes active area. Control of the size of the guide spot can be achieved through the placement of the wavefront sensor in relation to the image plane, hence by focussing or defocussing the telescope [14]. The guide spot must also present uniform light intensity in order to get an accurate measurement of its position. Inadequate considerations of these constraints will lead to undesirable performance of the overall system.

B. Control System Design

The control system was developed iteratively utilising a spiral software design approach, allowing modular functionality of the main individual components. The structure and requirements for the control system were identified in order to pin point the degrees of freedom and areas of focus for the development. The speed of the system was again the major design consideration that was the focus of optimisation through the design process.

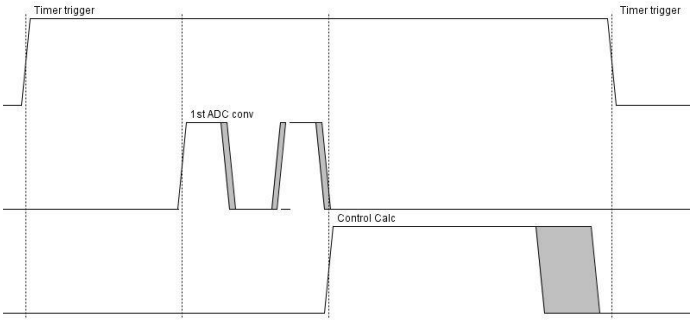

Figure 7: timing diagram of the controller system

1. Timing System

A constant timing system of appropriate frequency is vital to the accurate implementation of a control system [17]. Cooper (2008) identifies the minimum sampling time required is one tenth the value of the time constant of the control system. The time constant for a system (t_p) is defined as the time taken for the system to change the process variable in response to a change in the control output. This value needs to be derived with the plant in the control loop due to this parameter being highly dependent on the transfer function of the plant. The realisation of the timing system was achieved with the ATmega16U4 on-board timers triggered by the hardware interrupts. This provided a robust system that provided a timing system that exhibited negligible jitter. This method proved superior to the variants explored through implementation of the timing system within code. It also has the additional benefit of reducing the overhead of the data acquisition from the control system, allowing this functionality to be implemented outside of the main loop.

	Average (μs)	Jitter (μs)
ADC conversion	1^{st} 100 Then, 64	1
Timer trigger	Set to f_s	<1
Control calculation	170	14

Figure 8: Timing performance of control system components

2. Data acquisition

This implementation of the timing system allowed for the sampling of the wave front sensor to be implemented within the Interrupt Service Routine utilising the 10-bit on-board ADC. The timing performance of the ADC conversion was identified as a significant restriction on the speed of operation of the system. The speeds achieved (figure 7) match the quoted maximum achievable speed for the microprocessor [13]. As such without implementation of a different microprocessor this forms the ceiling of the system performance in terms of speed. The maximal operational speed was reduced to approximately 2.5 kHz. Attempts to optimise the

analogue read process were unsuccessful due to the optimised nature of the extant function provided. As such the inbuilt function was utilised for stability and performance consistency.

3. Control System

The control system was implemented through the generation of a PID controller class that was polled iteratively from the main loop of the program. The PID class implemented the algorithm shown in figure 2. Full design of the control system was unable to be conducted due to the tip/tilt mirror stage being unavailable due to breakages. As a result the framework to implement a control system was developed and coded, however the implementation of the control system has not yet been realised.

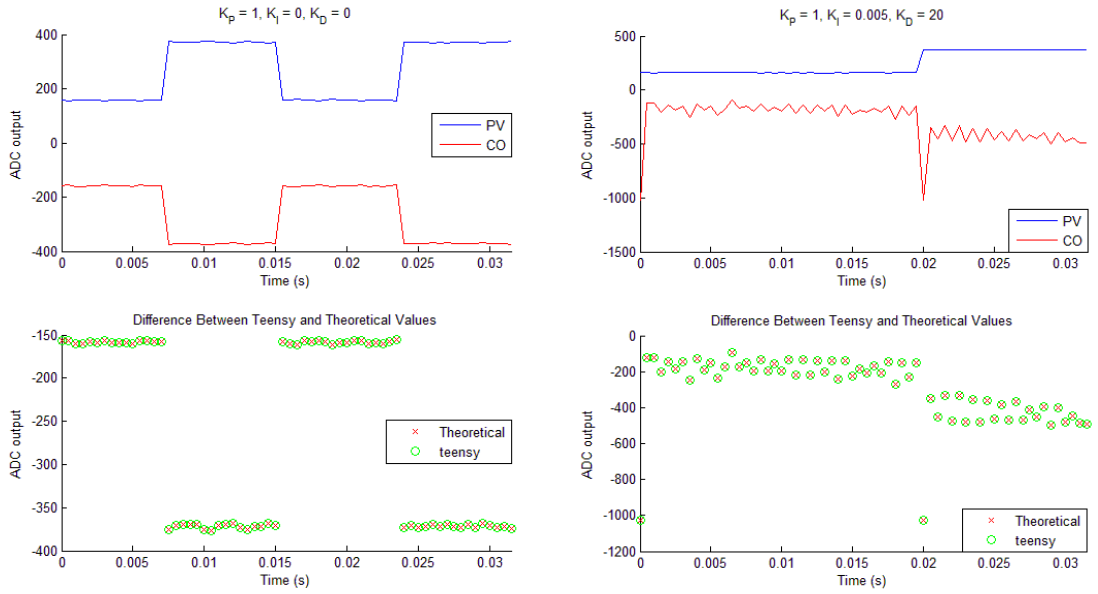

Figure 9: Controller performance confirmation: P (*left*), and PID (*right*). The implementation of the PID controller algorithm was tested by implementing a range of PID controller variants and comparing the Controller Output for the induced Process Variables against the theoretical response. This was realised through post processing the recorded Data in MATLAB.

Despite this, testing was conducted in order to ensure that the designed system was performing in the predicted and desired manner. This was identified as an important step in the design process as it provides confidence moving forward with the controller design that the controller implementation was sound. This was conducted by providing the control systems process variable with a square wave and recording the subsequent control output. The results were then reproduced and confirmed using MATLAB to ensure that the algorithm was sound and was providing the expected response. This is shown for three implementations of PID variant controllers in figure 9.

4. Data Collection

A vital component of the control system development was the ability to record the different parameters of the control system. This allowed the performance of the control system to be analysed and enabled the post processing of recorded data. However, the limited resources of the ATmega16U4 presented significant difficulties in attaining accurate results for the performance of the control system. The major limiting factor in terms of attaining sufficient data on the performance of the system was the memory available for saving the variables to prior to writing to the SD cart.

The overhead involved with the write operations for the SD card introduced significant latency into the system, resulting in numerous missed data points for any sampling frequencies above 10 Hz. This significantly impacted the performance of the control system and as such voided any results obtained after the SD write induced latency. In order to ensure this did not affect the data acquisition, the data to be recorded was initially written to on-board RAM and then dumped to the SD card in a single write operation. The memory constraints resulted in only 1024 bytes of memory being available for the raw data buffer. Whilst this restricted the sample size of the data, this was sufficient to test the controller algorithm (figure 9).The final realisation of data collection for the control system allows the Process Variables Control Outputs for the PID controller, or the raw quadrant outputs to be recorded. Memory use was optimised through the use of compile time code optimisation.

VII. Field Testing

Testing was conducted to jointly test the performance of the wave front sensor and to quantify the relative incoming wave front phase aberrations. This was achieved through the integration of the wave front sensor circuitry into the optical system and conducting measurements of the sensor output. Best results were observed during experiments conducted at night. This is due to a number of factors including; the significantly lower levels of turbulence experienced during the night hours, lower level of background light, and greater ease in which the target could be focused on the desired area of the wave front sensor. The recorded data exhibits the characteristics expected for the accurate performance of the wave front sensor, namely the complementary nature of opposing quadrants. It was observed that an increase in magnitude of a given quadrant is matched by a respective decrease in the opposing quadrant. This provides confidence that the recorded data is an accurate representation of the movement of the guide spot on the photodiode surface, and thus mapping of atmospheric distortion.

1. Test Setup

The field testing was conducted at the ADFA@UNSW Falcon telescope installation. The target LED was placed at a distance of 185m from the telescope at a height of 1.6m above the ground. The telescope was aligned utilising a Pulnix camera with fine alignment adjustments conducted by manipulating the position of the quadrature photodiode. Measurements of the four photodiode quadrants were recorded in order to be able to ensure correct performance of the wavefront sensor and to attain quantitative measurements of the levels of atmospheric distortion.

A number of important characteristics of the turbulence can be drawn from the results obtained; most prevalently the relative magnitude of distortion and the temporal evolution of this distortion. This information is important in the continued design of the system, as it indicates a measure of the distortion that the system must be capable of counteracting.

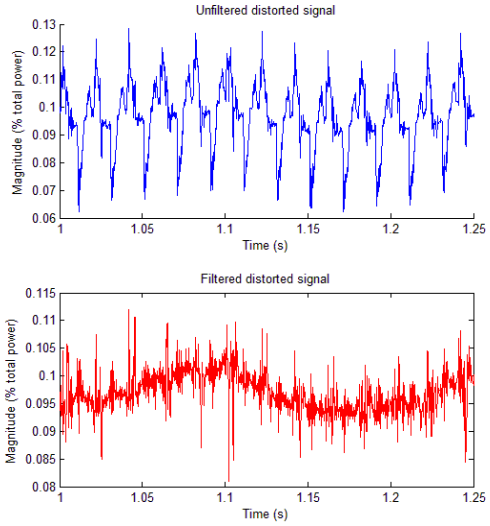

Figure 10: Use of comb filter to remove 50 Hz distortion

2. Input Normalisation

Of importance for both analysis of the data and the implementation as an input in the control system is the normalisation of the data to the gross received power. The gross received power exhibits temporal variation due to dynamic levels of background light. In order to be able to accurately compare successive wave front position sensor readings, these inputs must be expressed in terms of percentage of gross received power. Modelling this data allows for the average bias of the relative horizontal and vertical position to be established.

3. Noise in data

Of note in the analysis of the results is the presence of external noise in the measured data. This proved an issue extant in the measurements taken, with significant noise exhibited in the daytime measurements. Whilst this noise was later sourced to a ground leak into the telescope body due to the camera used to align the optical system, it is of use to demonstrate the use of filtering to recover the pertinent experimental data. This was achieved through the use of a comb filter. This approach has the effect of removing the identified sources of noise, but also has the potential to introduce unexpected behaviour into the results, as the presence of regular nulls in the frequency spectrum may introduce oscillations into the data itself. Any data in the raw signal at the frequencies removed by the comb filter are also lost.

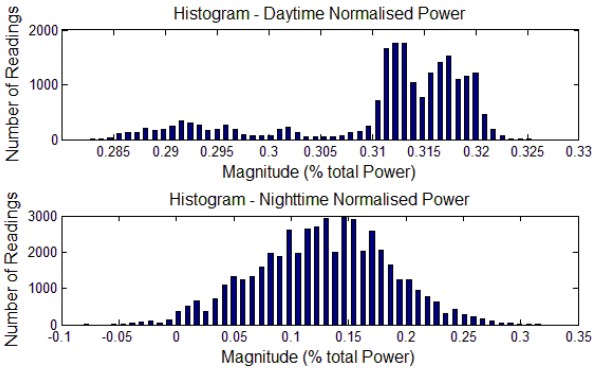

Figure 11: Distribution of daytime distortion (*top*), and night time distortion (*bottom*)

As such this method is useful in gaining an appreciation of the nature of the collected data, but all efforts to minimise the extant noise sources that affect the system performance were prioritised.

4. Distortion Magnitude

The relatively windless night time experiment produced favourable conditions for low levels of atmospheric turbulence, yet the quantitative distortion observed in the results differ between the vertical and horizontal distortions. It is observed that the distortion in the horizontal direction (parallel to the ground) was less than that in the Vertical direction (normal to the ground). This is indicative of the majority cause of distortion arising from atmospheric conditions propagating up from the ground, namely convection of heat from the ground still extant from warming during the day.

The data observed provides a good correlation to a normal distribution for the distortion for the night time testing. This indicates that the distortion present is distributed relatively evenly around a mean bias, with the bias indicates the average position of the guide object on the wave front sensor. As seen in figure 11 the distortion exhibited in the day time measurement cannot be modelled by a normal distribution. The histogram indicates that there are a number of superimposed sources of distortion that arise due to the daytime conditions. Analysing possible sources of this distortion is an area for future research.

Mapping the movement of the guide spot to the dimensions of the SPOT-4D photodiode allows for the quantitative level of correction required to be applied by the correctional mirror calculated. From this information the relative magnitude of correction required is able to be determined. For the night experiment it was found that the maximal distortion experienced was ±1mm for the vertical component and ±1.5mm for the horizontal component. As the correctional mirror removes the distortion by changing the length of the optical path, these values can be utilised to select a tip/tilt mirror with an appropriate stroke.

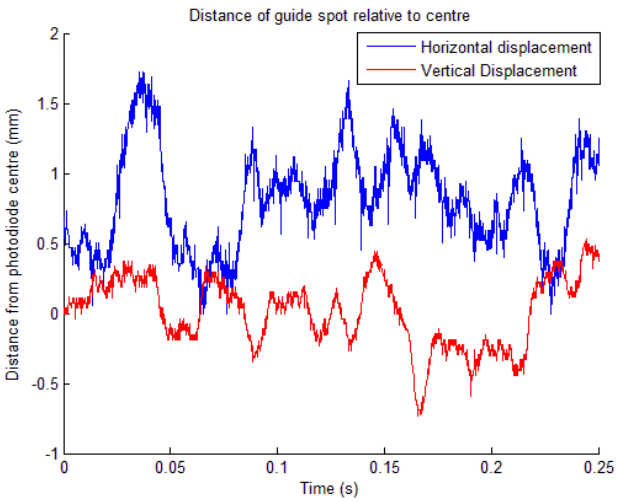

Figure 12: Mapping of distortion for night testing

5. Temporal Evolution

The temporal evolution of the distortion is what limits the speed of the overall system. The spectrograms in figure 13 show the quantitative temporal evolution of the atmospheric distortion for both daytime and night time testing. The magnitude of the incident light levels are seen to be significantly higher when compared to the night testing. The daytime testing also exhibits wide bands of distortion across the frequency, whereas the night time frequency spectra is more localised to the low frequencies with the presence of distinct frequencies. These distinct frequencies are unique to the night time measurements and as such are likely to be due to an environmental or test condition such as vibration of the source LED.

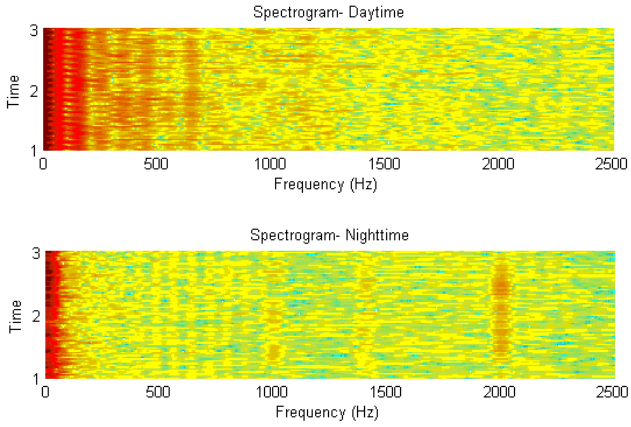

Figure 13: Spectrogram for atmospheric distortion during Daytime (*top*) and Night time measurements. Shows the prevalence of the frequency components of the distortion and how this distortion changed over time.

6. Non atmospheric sources of turbulence

There are a number of potential non-atmospheric sources of noise that could contribute to the measured level of distortion for the system. Of significance is the movement of the target itself throughout the sampling time. For the field testing conducted, the source LED was attached to a rigid plastic pole subsequently anchored to a

fence by threading the pole through the fence wires. This setup is noted to be prone to disturbance due to the wind. It is noted that this would present itself as each high frequency vibrations from the pole or low frequency oscillations in relationship to the anticipated evolution of atmospheric distortion, similar to the distortion observed in figure 13. Tichkule et al notes that vibrations induced by wind on similar optical systems to that utilised for this project experience wind induced vibrations proportional to the square of the wind speed [18]. This is noted to cause distortion exceeding two orders of magnitude greater than the background distortion, which is attempting to be measured [18]. Whilst this was not applicable to this testing due to the use of existing structure to shield the telescope it should be considered for future testing.

VIII. Conclusion

This project focussed on the design and development of an adaptive optics system for terrestrial surveillance. It was identified that due to the nature of the turbulence expected to be experienced in this implementation of adaptive optics that the speed of the system was the main design consideration to be optimised throughout the system development. Design of the first two components, the wave front sensor and control system, was successfully conducted with in depth analysis of sub system components characterised in order to determine the effect on system performance. A measure of the performance of the wave front sensor was achieved through integration onto the optical system platform, simultaneously confirming the operability of the sub system and providing valuable information on the nature of the turbulence present in terrestrial surveillance.

Testing of the wave front sensor provided accurate characterisation of the linearity, source of noise, effect of reverse bias and slew rate for the components of the system. An increase in reverse bias was shown to improve slew rate of the photodiode. The photodiode was shown to be linear when reverse biased within the tested range. The slew rate of the wave front sensor was shown to be proportional to the RC combination of the low pass filter in the biasing circuit.

A PID controller was designed utilising the ATmega16U4 microprocessor on the Arduino Teensy 2.0 microcontroller development board. Significant issues were encountered in the implementation of the control system due to the limited resources on the microcontroller. The physical control system was unable to be designed as the plant component was unable to be characterised due to breakage of the tip/tilt mirror that was to be implemented as the correctional mirror. The PID algorithm validated through testing for a range of PID controller implementations to enable future system integration and controller design.

Field testing proved the wavefront sensor was able to be integrated onto the extant optical platform without permanent or significant modifications to the telescope. This also provided quantitative data on the level of atmospheric distortion present which enables further design and implementation of the tip/tilt mirror stage of the system.

IX. Recommendations

The results obtained will allow future system development with the primary steps including the implementation of the correctional mirror to complete the control system. There is significant scope to conduct testing to determine the causes of variation between the characteristics of the atmospheric distortion observed in the results. However these are probably required to be conducted at the PhD level.

Acknowledgements

I would to acknowledge and thank my project supervisor, Dr Andrew Lambert SEIT UNSW@ADFA for his continued support and guidance throughout the project.

References

1. CoActionOs. 2014 [cited 2014 13 October]; Available from: http://coactionos.com/embedded%20design%20tips/2013/10/15/Tips-Motor-Control-using-PWM-and-PID/.
2. Technologies, O., *Adaptive Optics Guide*. Third ed. 2008, Delft Netherlands. 150.
3. Merkle, F., *Adaptive optics.* Physics World, 1991. **4**: p. 33-8.
4. Lambert, A., et al. *Turbulence profiling for long range surveillance imaging*. in *Optical Engineering+ Applications*. 2008. International Society for Optics and Photonics.
5. Vdovin, G., et al., *Correction of low order aberrations using continuous deformable mirrors.* Optics express, 2008. **16**(5): p. 2859-2866.
6. Platt, B.C., *History and principles of Shack-Hartmann wavefront sensing.* Journal of Refractive Surgery, 2001. **17**(5): p. S573-S577.
7. Kendrick, R.L., D.S. Acton, and A. Duncan, *Phase-diversity wave-front sensor for imaging systems.* Applied Optics, 1994. **33**(27): p. 6533-6546.
8. Katsuhiko, O., *Modern control engineering.* 2010.
9. Optoelectronics, O. *Photodiode Characteristics and Applications*. 2014.
10. OSIoptoelectronics *Segmented Photodiodes (SPOT series) datasheet*. 2014.
11. Thompson, L.A. and C.S. Gardner, *Experiments on laser guide stars at Mauna Kea Observatory for adaptive imaging in astronomy.* Nature, 1987. **328**(6127): p. 229-231.
12. PJRC. *Teensy USB Development Board*. 2014 [cited 2014 14 March]; Available from: https://www.pjrc.com/teensy/index.html.
13. *8-bit AVR Microcontroller with 16/32K Bytes of ISP Fash and USB Controller*, AVR, Editor. 2014.
14. Rousset, G., *Wave-front sensors.* Adaptive Optics in Astronomy, 1999. **1**: p. 91.
15. Tyson, R.K. and B.W. Frazier, *Field guide to adaptive optics*. Vol. 2. 2004: SPIE Press.
16. TL071, T.A., et al., *TL074B–Low noise JFET-input operational amplifiers.* Datasheet, Texas Instruments, 2005.
17. Cooper, D., *Practical Process Control-Proven Methods and Best Practices for Automatic PID Control*. 2008.
18. Tichkule, S. and A. Muschinski, *Effects of wind-driven telescope vibrations on measurements of turbulent angle-of-arrival fluctuations.* Applied optics, 2014. **53**(21): p. 4651-4660.